CHEMISTRY OF MATERIALS
Cite This: Chem. Mater. 2019, 31, 5699−5705
Article
pubs.acs.org/cm

Synthesis, Characterization, and Ultralow Thermal Conductivity of a Lattice-Mismatched $SnSe_2(MoSe_2)_{1.32}$ Heterostructure

Erik Hadland,[†] Hyejin Jang,[§] Matthias Falmbigl,[†] Robert Fischer,[†] Douglas L. Medlin,[‡] David G. Cahill,[§] and David C. Johnson*[,†]

[†]Department of Chemistry, Materials Science Institute, University of Oregon, Eugene, Oregon 97403, United States
[§]Department of Materials Science and Engineering and Materials Research Laboratory, University of Illinois, Urbana, Illinois 61822, United States
[‡]Sandia National Laboratories, Livermore, California 94551, United States

ABSTRACT: A significant experimental challenge in testing proposed relationships between structure and properties is the synthesis of targeted structures with atomistic control over both the structure and the composition. $SnSe_2(MoSe_2)_{1.32}$ was synthesized to test the hypothesis that the low-temperature synthesis of two interleaved structures would result in complete turbostratic disorder and that the disorder would result in ultralow thermal conductivity. $SnSe_2(MoSe_2)_{1.32}$ was prepared by depositing elements to form a precursor containing SnlSe and MolSe bilayers, each containing the number of atoms required to form single dichalcogenide planes. The nanoarchitecture of alternating Sn and Mo layers is preserved as the dichalcogenide planes self-assemble at low temperatures. The resulting compound contains well-formed dichalcogenide planes that closely resemble that found in the binary compounds and extensive turbostratic disorder. As expected from proposed structure−property relationships, the thermal conductivity of $SnSe_2(MoSe_2)_{1.32}$ is ultralow, ~0.05 W m^{-1} K^{-1}.

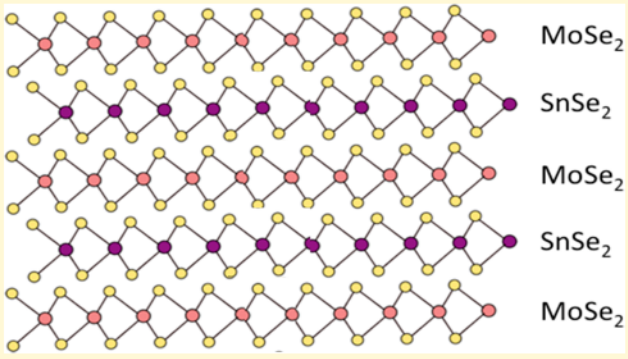

Exceptionally small thermal conductivities have been found in layered compounds with extensive turbostratic disorder (a random rotation or translation between adjacent basal planes).[1,2] The extent of turbostratic disorder is typically less than 100%, as an ordered crystal structure is thermodynamically favored.[3] Usually the extent of turbostratic disorder is controlled by processing conditions, with higher temperature and longer time annealing reducing the amount of disorder.[4] An alternative approach to maximize rotational disorder would be to choose different constituents in a heterostructure with a lattice mismatch that prevents the formation of a coherent interface between them.

Heterostructures with incommensurate interfaces, however, are usually thermodynamically unstable with respect to disproportionation and cannot be prepared by traditional synthesis approaches.[5] The approaches commonly used to prepare heterostructures, such as manual stacking of layers, yield small volumes of material, which can make characterizing the atomic structure and measuring physical properties challenging. It is hard to find common growth conditions for different constituents using van der Waals epitaxial growth techniques, so growing A on B and B on A is typically not possible.[5,6] An alternative approach that overcomes this problem is the modulated elemental reactant method, in which a precursor is prepared with the nanoarchitecture of the desired product.[7] Low-temperature annealing results in the self-assembly of the kinetically stable targeted product.

Here, we use this approach to test the hypothesis that lattice mismatch between two different hexagonal layers will maximize rotational disorder and result in exceptionally low thermal conductivity. We focus specifically on a target compound, $SnSe_2(MoSe_2)_{1.32}$, which would contain alternating layers of $SnSe_2$ and $MoSe_2$ with weak van der Waals bonding between them if it could be prepared (Figure 1). The large difference in the hexagonal basal plane lattice parameters between the two constituents, a = 0.381 nm for $SnSe_2$[8] and a = 0.329 nm for $MoSe_2$,[9−12] results in a misfit of 1.32. Therefore, the Se atoms in $SnSe_2$ cannot periodically reside in the middle of a Se triangle of the adjacent $MoSe_2$ layers. This should reduce the energy difference between different relative orientations, which we expect will result in extensive rotational disorder.

EXPERIMENTAL METHODS

The compound $SnSe_2(MoSe_2)_{1.32}$ was synthesized using the modulated elemental reactants (MER) technique.[2] Sn and Mo were deposited using electron beam guns, and Se was

Received: April 25, 2019
Revised: June 28, 2019
Published: July 8, 2019

DOI: 10.1021/acs.chemmater.9b01637
Chem. Mater. 2019, 31, 5699−5705

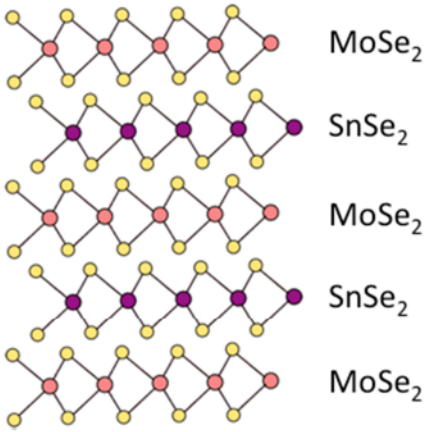

Figure 1. Schematic representation of the targeted $SnSe_2(MoSe_2)_{1.32}$ structure.

deposited using an effusion cell. All films were deposited on silicon wafers with a native oxide layer and on quartz substrates. Deposition was controlled using quartz crystal microbalances (QCM), and deposition rates were 0.1−0.3 Å/s. Shutters controlled the amount of each element deposited, and the order of deposition was determined by the sequence of shutter events. Precursors were annealed at various temperatures in a N_2 glovebox with a concentration of oxygen below 0.6 ppm to induce diffusion and self-assembly of the targeted product.

X-ray fluorescence spectroscopy was used to determine the number of atoms of each element deposited using a Rigaku ZSX Primus II wavelength-dispersive X-ray fluorescence spectrometer with a rhodium X-ray source. Intensity was measured by integrating the signal over the appropriate ranges for both the films and the substrates without any deposited film. The substrate-integrated counts were subtracted from the integrated intensity of the coated substrates to correct for the background. The proportionality constant between the XRF intensity and the atom density per unit area for each element was determined as previously described.[13]

Specular X-ray diffraction (XRD) scans were collected using a Bruker D8 Discover diffractometer equipped with Cu Kα radiation (λ = 0.15418 nm), a Göbel mirror, and Bragg−Brentano θ-2θ optics geometry. In-plane XRD was done on a Rigaku SmartLab diffractometer equipped with Cu Kα radiation in a grazing incidence geometry. High-quality in-plane XRD scans for Rietveld refinements were collected at the Advanced Photon Source at Argonne National Laboratories using beamline 33-C.

Cross-section specimens for transmission electron microscopy were prepared by standard focused ion beam (FIB) milling using a FEI Helios 600i Dual-Beam FIB. High-angle annular dark field scanning transmission electron microscopy (HAADF-STEM) and energy-dispersive X-ray spectroscopic (EDX) measurements were collected using a Themis Z instrument (FEI/Thermo Fisher Scientific) operated at 300 kV.

The van der Pauw technique[14] was used to measure electrical resistivity and Hall coefficients in a temperature range of 20−295 K. Samples were prepared on fused quartz crystal slides in a 1 cm × 1 cm cross geometry. Further details on how temperature-dependent resistivity and Hall measurements were conducted are described elsewhere.[15]

Thermal conductivity experiments were performed at room temperature using time-domain thermoreflectance as described previously.[16,17]

RESULTS AND DISCUSSION

We synthesized $SnSe_2(MoSe_2)_{1.32}$ by preparing a precursor that contained a repeating sequence of SeIMoISeISn elemental layers, where each SeIM bilayer contained the number of atoms required to form a single Se−M−Se trilayer of the respective dichalcogenide. The number of times the sequence was repeated controlled the number of unit cells that self-assembled and the thickness of the film. Annealing these films at 300 °C for 30 min in a dry N_2 atmosphere resulted in the self-assembly of the targeted structure. The low diffusion rates at this temperature prevented the precursor from disproportionating into a mixture of the thermodynamically more stable bulk constituents. Higher annealing temperatures resulted in the loss of Se and the formation of SnSe impurities. We found that a slight excess of Se (∼5%) increased the grain sizes in the resulting heterostructures. The resulting $SnSe_2(MoSe_2)_{1.32}$ films were annealed in a sealed tube with a Se partial pressure at 500 °C for 1 h to maximize Se occupancies in the respective dichalcogenides. The excess Se during annealing was condensed on the walls of the tube on cooling, resulting in stoichiometric films as measured using X-ray fluorescence.

The low-angle X-ray reflectivity (XRR) patterns of the annealed films, shown in Figure 2, contain the first two 00l

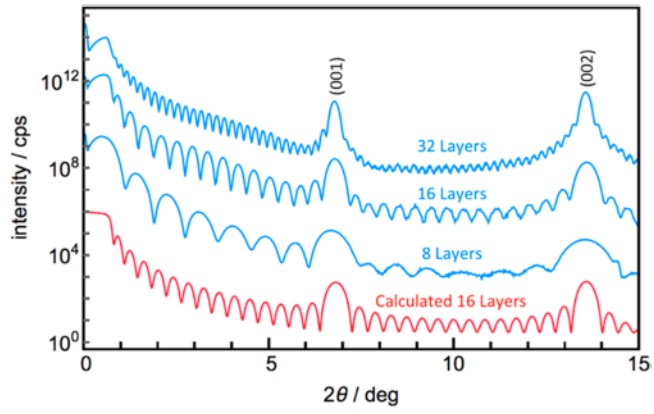

Figure 2. Representative XRR scans from a number of different $SnSe_2(MoSe_2)_{1.32}$ samples (blue traces), and calculated pattern (red trace) of the sample with 16 unit cells.

Bragg peaks of $SnSe_2(MoSe_2)_{1.32}$ and higher frequency intensity oscillations, which result from Kiessig fringes at low angles[18] and Laue oscillations at higher angles.[19] The position of the first two Bragg peaks are the same in the different films, indicating a constant c-axis lattice parameter (1.305(2) nm). The observation of oscillations to $2\delta > 15°$ indicates that the layers are smooth and parallel to one another within an Angstrom within the coherence length of the incident X-rays as determined by the Parratt relationship.[20] The total thickness calculated from the Kiessig fringes is an integral multiple of the c-axis lattice parameter. Each of the deposited layers self-assembles into a unit cell of the target structure. The agreement between the calculated and the experimental patterns indicates that the nanoarchitecture of the precursor is maintained in the final product.

DOI: 10.1021/acs.chemmater.9b01637
Chem. Mater. 2019, 31, 5699−5705

The structure of the heterostructures was also probed using high-angle specular (XRD) and in-plane diffraction (IPXRD) scans. All of the reflections in the specular XRD patterns (Figure 3) could be indexed as 00*l* reflections, yielding a *c*-axis

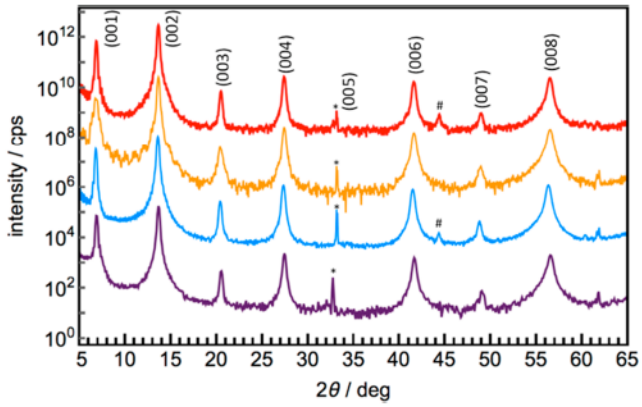

Figure 3. Four representative X-ray diffraction patterns of $SnSe_2(MoSe_2)_{1.32}$ samples; (00l) indices are shown above each reflection (* = substrate reflections, # = stage reflections).

lattice parameter of 1.307(5) nm for all films, in agreement with the XRR data. This lattice parameter is 0.05 nm larger than the sum of the $MoSe_2$ (0.646 nm)[9−12] and $SnSe_2$ (0.614 nm)[8,21] layers in their equilibrium bulk structures. This increase is larger than the 0.1 Å *c*-axis lattice parameter increase observed in turbostratically disordered $MoSe_2$ relative to crystalline $MoSe_2$.[3] The larger *c*-axis lattice parameter of $SnSe_2(MoSe_2)_{1.32}$ relative to the sum of the layer thicknesses found in the binary compounds may result from the lack of nesting of the Se atoms in adjacent layers as found in crystalline 2H $MoSe_2$.[9−12]

A representative in-plane X-ray diffraction pattern of an annealed $SnSe_2(MoSe_2)_{1.32}$ sample is shown in Figure 4. The

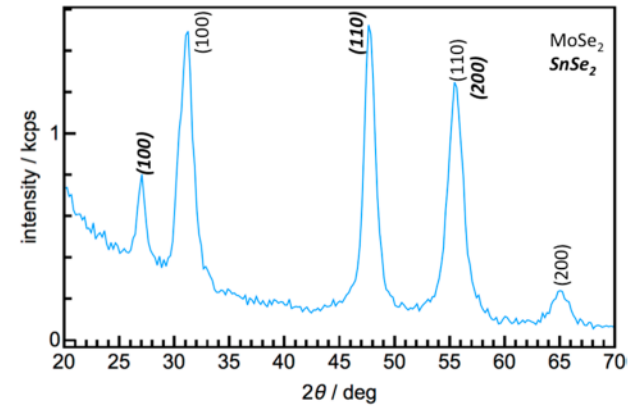

Figure 4. Representative in-plane diffraction pattern scan contains reflections that are consistent with two hexagonal lattices. Lattice parameters calculated from the indices of the *hk*0 maxima shown above the reflections match those of $SnSe_2$ and $MoSe_2$.

pattern contains maxima that can all be indexed as *hk*0 reflections of two different hexagonal lattices. The smaller *a*-axis lattice parameter [0.331(1) nm] is slightly larger than that reported for $MoSe_2$ (0.329 nm),[9−12] while the larger lattice parameter (a = 0.381(3) nm) matches that of $SnSe_2$ (a = 0.381 nm).[8] The in-plane diffraction data are consistent with the specular diffraction and reflectivity data, which are all consistent with a structure containing alternating layers of $SnSe_2$ and $MoSe_2$.

Atomic resolution HAADF-STEM data were collected from cross sections of the films to obtain more structural information. Figure 5 shows a representative cross section,

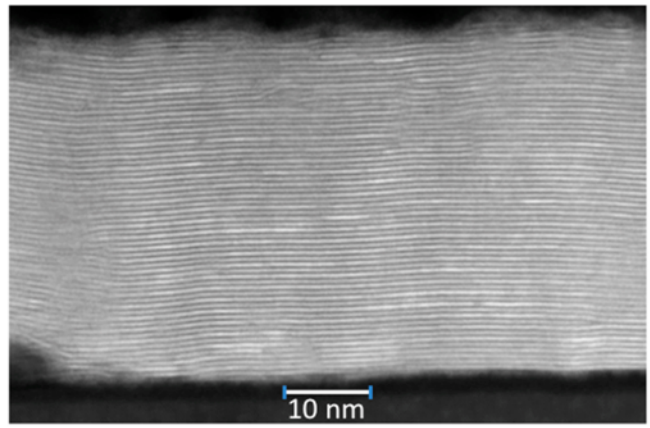

Figure 5. HAADF STEM images of a 32 unit cell thick $SnSe_2(MoSe_2)_{1.32}$ sample. Atomically smooth interfaces persist throughout the entire thickness of the sample.

from the top to the bottom of a sample containing 32 unit cells of $SnSe_2(MoSe_2)_{1.32}$. The higher atomic number of Sn relative to Mo should make planes containing Sn be brighter than layers containing Mo. There is little contrast between layers, however, due to the higher density of Mo atoms in $MoSe_2$ relative to Sn in $SnSe_2$, which offsets the difference in atomic number. There are atomically smooth interfaces between discrete layers, consistent with the diffraction data. We observed only a couple of small regions oriented along low-index zone axes.

Figure 6 shows a higher magnification image of a region with several low index zone axes visible within the same field-of-view. The different zone axis orientations in the respective layers are consistent with octahedral and trigonal prismatic coordination. There is a high degree of rotational disorder. Furthermore, within each layer the zone axis alignments persist for only 5−10 nm, providing a direct indication of the very small in-plane grain sizes.

Energy-dispersive X-ray spectroscopy (EDX) spectrum images were collected, and a representative region is shown in Figure 7. The intensity of Sn and Mo fluorescence alternates with a periodicity equal to the *c*-axis lattice parameter. Integrating the intensity over the area shown enabled us to determine the position of the atomic planes of Sn and Mo, which was used in the initial Rietveld refinement model described later. There is occasionally a spike of Mo intensity in the same location as the Sn maxima, for example, at $x \approx 13$ nm in Figure 6, suggesting that there may be some $MoSe_2$ regions in the $SnSe_2$ planes.

A Rietveld refinement was done on the specular diffraction pattern to obtain the distances between atomic planes along the *c* axis. Since only 00*l* reflections are observed, the diffraction data is not sensitive to symmetry within the $x-y$ plane.[22] Mirror planes perpendicular to the *c* axis on the planes of the cations of the dichalcogenide structural unit were assumed. The atomic densities were initially assumed to be identical to the binary compounds. Figure 8 shows the

DOI: 10.1021/acs.chemmater.9b01637
Chem. Mater. 2019, 31, 5699−5705

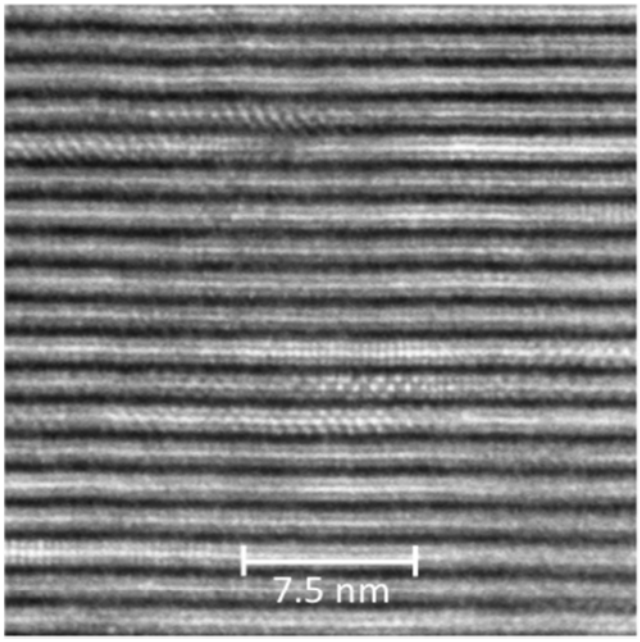

Figure 6. Higher magnification HAADF STEM image showing a rare region where several low index zone axes are visible. Lack of long-range alignment of the zone axes is consistent with turbostratic disorder.

refinement of a specular diffraction pattern where the relative positions of the atomic planes of Mo, Sn, and Se determined from STEM-EDS data were used as an initial model. The refined distance between Mo and Se planes within a $MoSe_2$ layer of $SnSe_2(MoSe_2)_{1.32}$, 0.166(1) nm, is consistent with that reported for $MoSe_2$ (0.1667 nm).[9−12] To get a reasonable refinement, some of the Mo that was within the Sn plane of the $SnSe_2$ layer was required, which was suggested by the EDX and in-plane diffraction data (discussed next). The resulting occupancies (8% Mo, 92%Sn (±5%)) are consistent with XRF and STEM EDS data. Rather than being a random substitution, the EDX data and in-plane diffraction data discussed in the following paragraph both suggest that there are regions of $MoSe_2$ within the $SnSe_2$ layer. The spacing between Sn and Se planes in the $SnSe_2$ layer in $SnSe_2(MoSe_2)_{1.32}$, 0.157(1) nm, is slightly larger than that reported for $SnSe_2$(0.153 nm).[8,19] The refined van der Waals gap between the $SnSe_2$ and the $MoSe_2$ constituents, 0.335(1) nm, is 0.023 nm larger than that found in $MoSe_2$ and 0.029 nm larger than the van der Waals gaps in $SnSe_2$. We speculate that this expansion is a result of the inability of adjacent layers to settle (or nest) within each other as found in 2H or 3R $MoSe_2$ and is indicative of turbostratic disorder.

The results of refining the in-plane diffraction pattern of $SnSe_2(MoSe_2)_{1.32}$ are shown in Figure 9. The structures of the different dichalcogenide layers were assumed to be identical to that of the bulk binary compounds, and the space groups for the bulk solids were used in the refinement.[8−12] The atoms are all on special position sites in both structures; there were no x and y coordinates to refine. The z coordinates of the atoms do not change the intensity of the $hk0$ reflections. Reasonable refinements were obtained with all atoms constrained to the special position sites, refining the lattice parameters and the relative scattering of the different lattices. The agreement between the measured and the calculated intensity indicates that layers have the structures of the respective binary

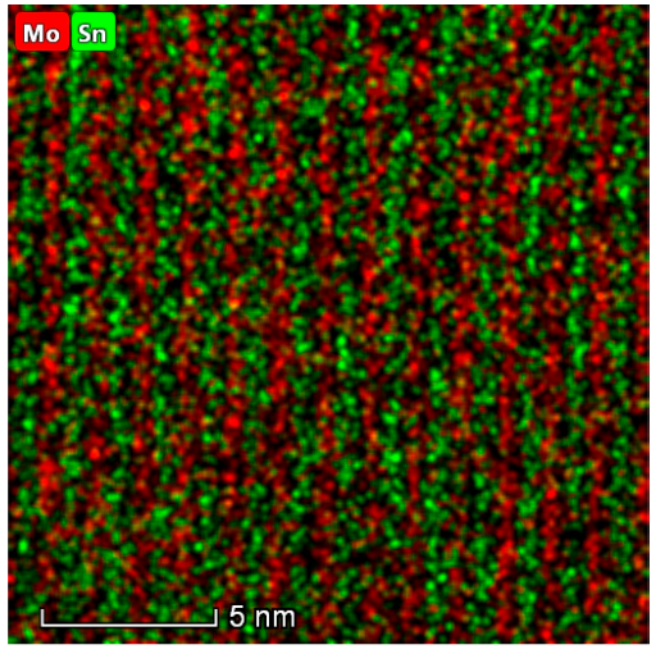

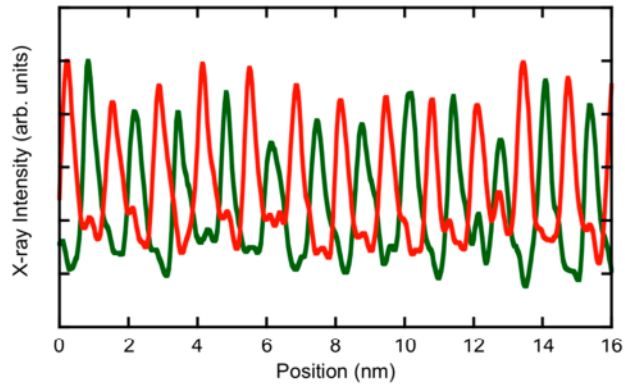

Figure 7. EDX spectrum image of a region of the $SnSe_2(MoSe_2)_{1.32}$. Lower graph plots the variation of the intensity of characteristic X-rays for Mo and Sn versus the distance along the c axis, obtained by integrating the EDX spectrum image in the direction parallel to the layers.

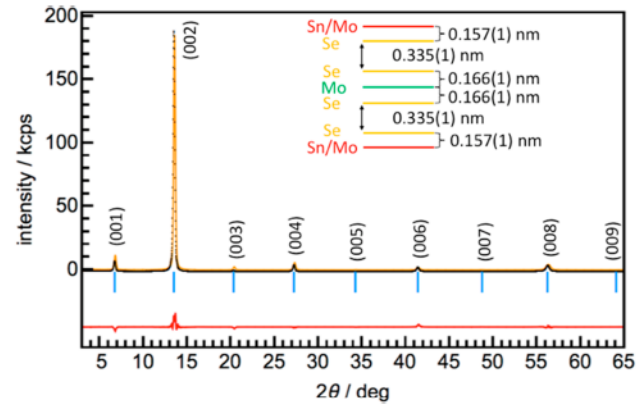

Figure 8. Rietveld refinement of the specular diffraction pattern of $SnSe_2(MoSe_2)_{1.32}$ using initial positions of the atomic planes derived from STEM and STEM EDX data. (Inset) Distance between atomic planes determined from the refinement.

DOI: 10.1021/acs.chemmater.9b01637
Chem. Mater. 2019, 31, 5699−5705

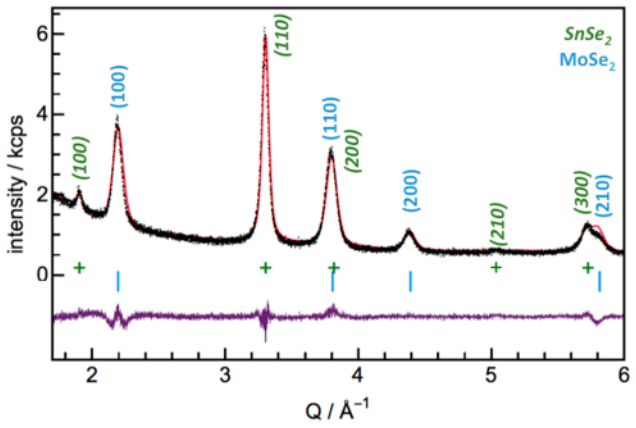

Figure 9. Rietveld refinements of the in-plane diffraction pattern of $SnSe_2(MoSe_2)_{1.32}$ with all of the atom positions constrained to the special sites found in the respective binary compounds. Relative intensity of the $MoSe_2$ pattern is higher than expected.

compounds. The *a*-axis lattice parameters [0.331(1) and 0.381(3) nm] match those reported for $MoSe_2$ (0.329 nm) and $SnSe_2$ (a = 0.381 nm),[8−12] suggesting the relative amount of substitution of Mo in $SnSe_2$ or Sn in $MoSe_2$ is small. The relative intensity of the $MoSe_2$ constituent, however, is 20% ± 10% higher than expected based on the misfit parameter. The agreement of the *a*-axis lattice parameters with the bulk compounds, the higher relative intensity of the $MoSe_2$ in the refinement of the in-plane diffraction pattern, needing Mo in the Sn layer to refine the specular diffraction pattern and the spikes of Mo intensity found in some of the Sn planes in the STEM EDX data are all consistent with occasional domains of $MoSe_2$ in the $SnSe_2$ planes.

Electrical resistivity data was obtained using the van der Pauw method. The resistivity increased from 0.067 Ω m at 295 K to 2.35 Ω m at 150 K. A linear regression of ln ρ versus T^{-1} yielded an activation energy of 0.20(3) eV over this small temperature range, Figure 10, which is significantly smaller than the reported band gaps of monolayer $MoSe_2$ (∼1.55 eV),[23−25] bulk $MoSe_2$ (∼1.4 eV),[26] or $SnSe_2$ (∼0.8−1.1 eV).[27−29] The small activation energy may result from activation to or from a dopant band or grain boundary depletion due to the small in-plane grain sizes. An alternative explanation is that there is a type II alignment of the bands and

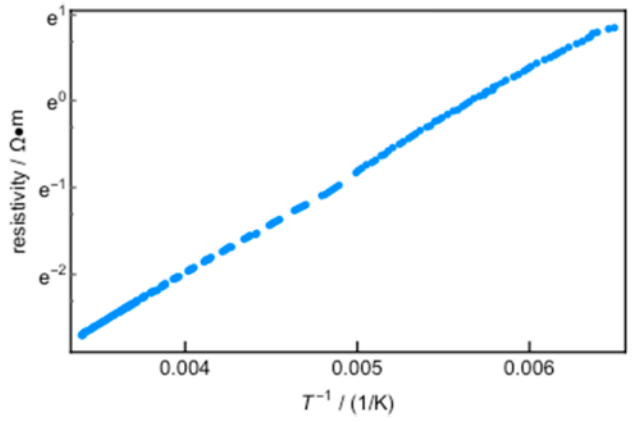

Figure 10. Graph of ln ρ versus inverse temperature. Linear relationship is consistent with an activated conductivity. Errors of the measured values are less than the size of the data points.

the activation energy is that of an interlayer band gap. This would be consistent with a calculation for a $SnSe_2/MoSe_2$ heterostructure, which yielded an interlayer band gap of 0.1 eV.[30]

Cross-plane thermal conductivity was measured with time-domain thermal reflectance (TDTR). The thermal conductivities varied from 0.04 W m^{-1} K^{-1} for the thinnest film containing 8 $SnSe_2(MoSe_2)_{1.32}$ unit cells to 0.06 W m^{-1} K^{-1} for a film containing 32 $SnSe_2(MoSe_2)_{1.32}$ unit cells (Table 1).

Table 1. Summary of Lattice Parameters and Cross-Plane Thermal Conductivity (Λ) for $SnSe_2(MoSe_2)_{1.32}$ Films with Different Thicknesses[a]

no. of unit cells in film	$SnSe_2$ a (nm)	$MoSe_2$ a (nm)	c (nm)	Λ (W m^{-1} K^{-1})
32	0.381(1)	0.311(1)	1.307(1)	0.06(1)
16	0.381(1)	0.311(1)	1.303(1)	0.05(1)
8	0.381(1)	0.310(1)	1.302(6)	0.04(1)

[a]Errors are given in parentheses.

These values are similar to those reported for turbostratically disordered WSe_2, i.e., 0.05 W m^{-1} K^{-1} at room temperature, the lowest value reported for any fully dense solid.[1] These values are slightly smaller than the thermal conductivity of turbostratically disordered $MoSe_2$, 0.07−0.09 W m^{-1} K^{-1}.[3] The reported conductivity is significantly lower than the cross-plane thermal conductivity of $MoSe_2$ single crystals (∼3 W m^{-1} K^{-1})[31] or $SnSe_2$ single crystals (∼1.4 W m^{-1} K^{-1}).[19] The ultralow thermal conductivity of $SnSe_2(MoSe_2)_{1.32}$ films can be attributed to the fact that rotational disorder effectively suppresses the group velocity of transverse phonon modes.[3] Low thermal conductivities (0.1−0.3 W m^{-1} K^{-1}) were previously reported for a number of different dichalcogenides prepared using magnetron sputtering, but these samples had extensive structural disorder not found in the films studied herein.[32]

CONCLUSIONS

This study shows that interleaving two structures with significant lattice mismatch results in turbostratic disorder between the constituent layers and lowers thermal conductivity to ultralow values. The detailed structural characterization shows that the heterostructure is highly periodic containing alternating, well-formed and planar $MoSe_2$ and $SnSe_2$ monolayers that retain the in-plane structure of their bulk lattices. The large mismatch between basal plane structures maximizes rotational disorder and also increases the van der Waals gap in the heterostructures. The interplanar rotational disorder gives rise to highly anisotropic bonding environments for the Se atoms in both constituent layers, as they no longer reside in high-symmetry sites. The synthesis of the metastable compound $SnSe_2(MoSe_2)_{1.32}$, which is unstable at high temperatures, was accomplished using designed precursors. The precursors had a controlled number of atoms per unit area, alternated in a designed sequence, which matched that of the desired product. Annealing the precursor self-assembled the targeted compound at relatively low temperatures. Since this synthesis approach is not based on epitaxy, it is widely applicable to heterostructures containing constituents with greatly dissimilar chemistries and crystal structures.

DOI: 10.1021/acs.chemmater.9b01637
Chem. Mater. 2019, 31, 5699−5705

AUTHOR INFORMATION

Corresponding Author

*E-mail: davej@uoregon.edu.

ORCID

David C. Johnson: 0000-0002-1118-0997

Author Contributions

The manuscript was written through contributions of all authors.

Notes

The authors declare no competing financial interest.

ACKNOWLEDGMENTS

The authors acknowledge support from the National Science Foundation under grant DMR-1710214. We also acknowledge the Center for Advanced Materials Characterization in Oregon (CAMCOR) at the University of Oregon. We thank Jenia Karapetrova for assistance at Beamline 33-C at the Advanced Photon Source (APS) in Argonne National Laboratories. The use of the APS was supported by the U.S. Department of Energy, Office of Science, and the Office of Basic Energy Sciences, under Contract No. DE-AC02-06CH11357. Sandia National Laboratories is a multimission laboratory managed and operated by National Technology and Engineering Solutions of Sandia, LLC, a wholly owned subsidiary of Honeywell International Inc. for the U.S. Department of Energy's National Nuclear Security Administration under contract DE-NA-0003525.

ABBREVIATIONS

XRF, X-ray fluorescence; XRD, X-ray diffraction; HAADF-STEM, high-angle annular dark field scanning transmission electron microscopy

REFERENCES

(1) Chiritescu, C.; Cahill, D. G.; Nguyen, N.; Johnson, D. C.; Bodapati, A.; Keblinski, P.; Zschack, P. Ultralow Thermal Conductivity in Disordered, Layered WSe_2 Crystals. *Science* **2007**, *315*, 351−353.

(2) Gunning, N. S.; Feser, J.; Beekman, M.; Cahill, D. G.; Johnson, D. C. Synthesis and Thermal Properties of Solid-State Structural Isomers: Ordered Intergrowths of SnSe and $MoSe_2$. *J. Am. Chem. Soc.* **2015**, *137*, 8803−8809.

(3) Hadland, E. C; Jang, H.; Wolff, N.; Fischer, R.; Lygo, A. C; Mitchson, G.; Li, D.; Kienle, L.; Cahill, D. G; Johnson, D. C Ultralow Thermal Conductivity of Turbostratically Disordered $MoSe_2$ Ultra-Thin Films and Implications for Heterostructures. *Nanotechnology* **2019**, *30*, 285401.

(4) Zheng, T.; Reimers, J. N.; Dahn, J. R. Effect Of Turbostratic Disorder In Graphitic Carbon Hosts On The Intercalation Of Lithium. *Phys. Rev. B: Condens. Matter Mater. Phys.* **1995**, *51*, 734.

(5) Lotsch, B. V. Vertical 2D Heterostructures. *Annu. Rev. Mater. Res.* **2015**, *45*, 85−109.

(6) Chen, P.; Zhang, Z.; Duan, X.; Duan, X. Chemical Synthesis of Two-dimensional Atomic Crystals, Heterostructures and Superlattices. *Chem. Soc. Rev.* **2018**, *47*, 3129−3151.

(7) Esters, M.; Johnson, D. C. Targeted Synthesis of Metastable Compounds and Intergrowths: the Modulated Elemental Reactants Method. In *Crystal Growth: Concepts, Mechanisms and Applications*; Li, J., Li, J., Chu, Y., Eds.; Nova Publishers: Hauppauge, NY, 2017; Chapter 2.

(8) Pałosz, B.; Salje, E. Lattice Parameters and Spontaneous Strain in AX_2Polytypes: CdI_2, PbI_2 SnS_2 and $SnSe_2$. *J. Appl. Crystallogr.* **1989**, *22*, 622−623.

(9) Evans, B. L.; Hazelwood, R. A. Optical and Structural Properties of $MoSe_2$. *Phys. Status Solidi* **1971**, *4*, 181−192.

(10) Kalikhman, V. L. Characteristics of the Crystal Structure, Electrophysical Properties, And Model of the Valence Band Spectrum of Laminar Compounds of Molybdenum Disulfide Type. *Inorg. Mater.* **1983**, *19*, 957−962.

(11) Brixner, L. H. Preparation and Properties of the Single Crystalline AB_2-Type Selenides And Tellurides of Niobium, Tantalum, Molybdenum and Tungsten. *J. Inorg. Nucl. Chem.* **1962**, *24*, 257−263.

(12) Bronsema, K. D.; De Boer, J. L.; Jellinek, F. On the Structure of Molybdenum Diselenide and Disulfide. *Z. Anorg. Allg. Chem.* **1986**, *540*, 15−17.

(13) Hamann, D. M.; Bardgett, D.; Cordova, D. L. M.; Maynard, L. A.; Hadland, E. C.; Lygo, A. C.; Wood, S. R.; Esters, M.; Johnson, D. C. Sub-monolayer Determination of the Number of Atoms Per Unit Area in Ultrathin Films Using X-ray Fluorescence. *Chem. Mater.* **2018**, *30*, 6209−6216.

(14) van der Pauw, L. J. A Method of Measuring Specific Resistivity and Hall Effect of Discs of Arbitrary Shape. *Philips Res. Rep.* **1958**, *13*, 1−11.

(15) Alemayehu, M. B.; Mitchson, G.; Ditto, J.; Hanken, B. E.; Asta, M.; Johnson, D. C. Charge Transfer between PbSe and $NbSe_2$ in $[(PbSe)_{1.14}]_m(NbSe_2)_1$Ferecrystalline Compounds. *Chem. Mater.* **2014**, *26*, 1859−1866.

(16) Cahill, D. G. Analysis Of Heat Flow In Layered Structures For Time-Domain Thermoreflectance. *Rev. Sci. Instrum.* **2004**, *75*, 5119−5122.

(17) Costescu, R. M.; Wall, M. A.; Cahill, D. G. Thermal Conductance Of Epitaxial Interfaces. *Phys. Rev. B* **2003**, *67*, 054302.

(18) Kiessig, H. Interferenz von Röntgenstrahlen an dünnenSchichten. *Ann. Phys.* **1931**, *402*, 769.

(19) Warren, B. *X-Ray Diffraction*; Dover: New York, 1990.

(20) Wainfan, N.; Parratt, L. G. X-Ray Reflection Studies of the Anneal and Oxidation of Some Thin Solid Films. *J. Appl. Phys.* **1960**, *31*, 1331−1337.

(21) Busch, A.; Fröhlich, C.; Hulliger, C.; Steigmeier, E. Struktur, Elektrische und ThermoelektrischeEigenschaften von $SnSe_2$. *Helv. Phys. Acta* **1961**, *34*, 359−368.

(22) Smeller, M. M.; Heideman, C. L.; Lin, Q.; Beekman, M.; Anderson, M. D.; Zschack, P.; Anderson, I. M.; Johnson, D. C. Structure of Turbostratically Disordered Misfit Layer Compounds $[(PbSe)_{0.99}]_1[WSe_2]_1$, $[(PbSe)_{1.00}]_1[MoSe_2]_1$, and $[(SnSe)_{1.03}]_1[MoSe_2]_1$. *Z. Anorg. Allg. Chem.* **2012**, *638*, 2632−2639.

(23) Mann, J.; Ma, Q.; Odenthal, P. M.; Isarraraz, M.; Le, D.; Preciado, E.; Barroso, D.; Yamaguchi, K.; von Son Palacio, G.; Nguyen, A.; Tran, T.; Wurch, M.; Nguyen, A.; Klee, V.; Bobek, S.; Sun, D.; Heinz, T. F.; Rahman, T. S.; Kawakami, R.; Bartels, L. 2-Dimensional Transition Metal Dichalcogenides with Tunable Direct Band Gaps: $MoS_{2(1-x)}Se_{2x}$ Monolayers. *Adv. Mater.* **2014**, *26*, 1399−1404.

(24) Tongay, S.; Narang, D. S.; Kang, J.; Fan, W.; Ko, C.; Luce, A. V.; Wang, K. X.; Suh, J.; Patel, K. D.; Pathak, V. M.; Li, J.; Wu, J. Two-Dimensional Semiconductor Alloys: Monolayer $Mo_{1-x}W_xSe_2$. *Appl. Phys. Lett.* **2014**, *104*, 012101.

(25) Tongay, S.; Zhou, J.; Ataca, C.; Lo, K.; Matthews, T. S.; Li, J.; Grossman, J. C.; Wu, J. Thermally Driven Crossover From Indirect Toward Direct Bandgap In 2D Semiconductors: $MoSe_2$Versus MoS_2. *Nano Lett.* **2012**, *12*, 5576−5580.

(26) Kim, B. S.; Rhim, J.; Kim, B.; Kim, C.; Park, S. R. Determination Of The Band Parameters Of Bulk 2H-MX_2 (M = Mo, W; X = S, Se) By Angle-Resolved Photoemission Spectroscopy. *Sci. Rep.* **2016**, *6*, 36389.

(27) Martínez-Escobar, D.; Ramachandran, M.; Sánchez-Juárez, A.; Narro Rios, J. S. Optical And Electrical Properties Of $SnSe_2$ and SnSeThin Films Prepared By Spray Pyrolysis. *Thin Solid Films* **2013**, *535*, 390−393.

(28) Fernandes, P. A.; Sousa, M. G.; Salomé, P. M. P.; Leitão, J. P.; Da Cunha, A. F. Thermodynamic Pathway For The Formation Of

DOI: 10.1021/acs.chemmater.9b01637
Chem. Mater. 2019, 31, 5699−5705

SnSe and $SnSe_2$ Polycrystalline Thin Films By Selenization Of Metal Precursors. *CrystEngComm* **2013**, *15*, 10278.
(29) Gonzalez, J. M.; Oleynik, I. I. Layer-Dependent Properties Of SnS_2 and $SnSe_2$Two-Dimensional Materials. *Phys. Rev. B: Condens. Matter Mater. Phys.* **2016**, *94*, 125443.
(30) Chen, P.; Shang, J.; Yang, Y.; Wang, R.; Cheng, X. Annealing Tunes Interlayer Coupling And Optoelectronic Property Of Bilayer $SnSe_2$/$MoSe_2$Heterostructures. *Appl. Surf. Sci.* **2017**, *419*, 460−464.
(31) Jiang, P.; Qian, X.; Gu, X.; Yang, R. Probing Anisotropic Thermal Conductivity of Transition Metal Dichalcogenides MX_2 (M = Mo, W and X = S, Se) Using Time-Domain Thermoreflectance. *Adv. Mater.* **2017**, *29*, 1701068.
(32) Muratore, C.; Varshney, V.; Gengler, J. J.; Hu, J. J.; Bultman, J. E.; Smith, T. M.; Shamberger, P. J.; Qiu, Bo; Ruan, X.; Roy, A. K.; Voevodin, A. A. Cross-Plane Thermal Properties Of Transition Metal Dichalcogenides. *Appl. Phys. Lett.* **2013**, *102*, 081604.

DOI: 10.1021/acs.chemmater.9b01637
Chem. Mater. 2019, 31, 5699−5705